Development of scalable Discontinuous Galerkin solvers for time- and frequency-domain electromagnetics and nanophotonics

Stéphane Lanteri

International Workshop on High Performance Computing
for Electromagnetic and Multiphysics Modeling
International Campus, Zhejiang University, Haining
May 11-13, 2017

Outline

1. Context
2. Time-domain modeling
   - Brief history of the development of DGTD methods
   - DGTD methods for nanoscale light/matter interactions
3. Frequency-domain modeling
   - Hybridizable DG method
   - Scalable DD-based HDG solver
4. Closure

Who are we ?

Inria: French national institute for computer science and applied mathematics

Scientific objectives

- Methodology-driven team
- Key disciplines: applied mathematics and scientific computing
- Numerical modeling of physical problems involving waves in interaction with complex media and irregularly shaped structures
  - Time-domain and frequency-domain wave propagation problems
  - Elctromagnetics and elastodynamics
  - Applications: nanophotonics/nanoplasmonics
- Contributions
  - Theoretical (properties of numerical methods)
  - Practical (numerical algorithms and associated software)

Research directions

1. High order geometry conforming finite element type methods
2. Solution strategies for multiscale problems
3. Architecture-aware algorithms for high performance computing architectures

Context

- Somewhere between a finite element and a finite volume method, gathering many good features of both
- Extensively developed by the CFD community
- Application to wave propagation problems naturally followed
- J.S. Hesthaven and T. Warburton (Springer, 2008)
  Nodal discontinuous Galerkin methods: algorithms, analysis, and applications

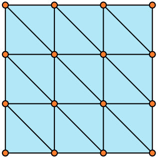

(a) Finite elements: continuous, non-constant-per-cell solution

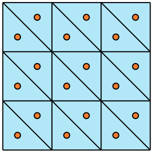

(b) Finite volumes: discontinuous, constant-per-cell solution

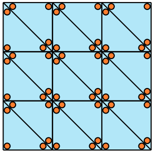

(c) Discontinuous Galerkin: discontinuous, non-constant-per-cell solution

DG for electromagnetic wave propagation in heterogeneous media

- Heterogeneity is ideally treated at the element level
  - Discontinuities occur at material (i.e element) interfaces
  - Mesh generation process is simplified
- Wavelength varies with ε and μ
  - For a given mesh density, approximation order can be adapted at the element level in order to fit to the local wavelength

Discretization of irregularly shaped domains

- Unstructured simplicial meshes
- The basic support of the DG method is the element (triangle in 2D and tetrahedron in 3D)
- Local refinement is facilitated by allowing non-conformity
- Non-conformity opens the route to the coupling of different discretization methods (e.g structured/unstructured)
- For time-domain problems, mass matrix is block diagonal (worst case) or diagonal (J. Xin and W. Cai, J. Sci. Comput., Vol. 50, 2012)

1. Context

2. Time-domain modeling
   - Brief history of the development of DGTD methods
   - DGTD methods for nanoscale light/matter interactions

3. Frequency-domain modeling
   - Hybridizable DG method
   - Scalable DD-based HDG solver

4. Closure

Outline

1. Context
2. Time-domain modeling
   - Brief history of the development of DGTD methods
   - DGTD methods for nanoscale light/matter interactions
3. Frequency-domain modeling
   - Hybridizable DG method
   - Scalable DD-based HDG solver
4. Closure

Brief history of the development of DGTD methods

- F. Bourdel, P.A. Mazet and P. Helluy
  Proc. 10th Inter. Conf. on Comp. Meth. in Appl. Sc. and Eng., 1992.
  - Triangular meshes, first-order upwind DG method (i.e FV method)
  - Time-domain and time-harmonic Maxwell equations
- M. Remaki and L. Fezoui, Inria Reserach Report RR-3501, 1998.
  - Time-domain Maxwell equations
  - Triangular meshes, P1 interpolation, Runke-Kutta time integration (RKDG)
- J.S. Hesthaven and T. Warburton (J. Comput. Phys., Vol. 181, 2002)
  - Tetrahedral meshes, high order Lagrange polynomials, upwind flux
  - Runge-Kutta time integration
- B. Cockburn, F. Li and C.-W. Shu (J. Comput. Phys., Vol. 194, 2004)
  - Locally divergence-free RKDG formulation
- G. Cohen, X. Ferrieres and S. Pernet (J. Comput. Phys., Vol. 217, 2006)
  - Hexahedral meshes, high order Lagrange polynomials, penalized formulation
  - Leap-frog time integration scheme

Brief history of the development of DGTD methods

- V. Kabakian, V. Shankar and W.F. Hall (J. Sci. Comput., Vol. 20, 2004)
  - Upwind flux
  - Monomial polynomials
  - Runge-Kutta time integration scheme
- T. Lu, P.W. Zhang and W. Cai (J. Comput. Phys., Vol. 200, 2004)
  - Dispersive medium (Debye), ADE technique
  - Perfectly Matched Layers (UPML)
  - Hybrid quadrangular/triangular meshes
  - Upwind flux
  - Runge-Kutta time integration scheme
- M.H. Chen, B. Cockburn and F. Reitich (J. Sci. Comput., Vol. 22-23, 2005)
  - Strong stability preserving Runge-Kutta time integration schemes
  - Post-processing techniques to double the convergence order
- And a steadily increasing number of other works and groups adopting the method since 2005

Brief history of the development of DGTD methods

ElectroScience Laboratory, The Ohio State University, USA

- Jin-Fa Lee *et al.*

- Interior penalty discontinuous Galerkin formulation
- Triangular (2D)/tetrahedral meshes, conformal PMLs
- Leap-frog time integration scheme, local time-stepping strategy
  - S. Dosopoulos and J.F. Lee
    IEEE Trans. Ant. Propag., Vol. 58, 2010
  - S. Dosopoulos and J.F. Lee
    J. Comput. Phys., Vol. 229, 2010

By courtesy of J.F. Lee

Computational Electromagnetics Group TU Darmstadt, Germany

- S. Schnepp, T. Weiland *et al.*
- Non-dissipative (centered flux) discontinuous Galerkin formulation
- Orthogonal quadrangular (2D)/hexahedral (3D) meshes
- Adpative mesh refinement
- Leap-frog time integration scheme
  - S. Schnepp and T. Weiland Radio Science, Vol. 46, 2011

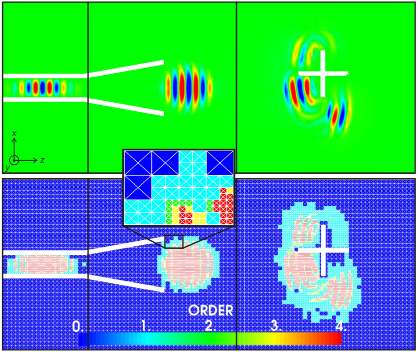

By courtesy of S. Schnepp

Brief history of the development of DGTD methods

- J. Alvarez, L.D. Angulo, A.R. Bretones and S.G. Garcia (IEEE Trans. Microw. Theory Tech., Vol. 60, No. 8, 2012)
  - Spurious-free DGTD method
  - Study of the role of the penalization parameter with upwind flux
- J. Alvarez, L.D. Angulo, A.R. Bretones and S.G. Garcia (IEEE Ant. Wir. Prop. Lett., Vol. 11, 2012)
  - 3D anisotropic materials
  - Upwind flux based on solutoin of Riemann problem
- S. Yan and J. Jin (IEEE Trans. Ant. Propag, Vol. 65, No. 5, 2017)
  - Electromagnetic and multiphysics problems
  - Dynamic adaptation of the interpolation order (p-adaptivity)
  - Based on cheap error estimator
- C.P. Chang, G. Chen, S. Yan and J. Jin (Int. J. Numer. Model., Electron. Netw. Devices Fields, Vol. 65, No. 5, 2017)
  - Waveport boundary condition (WPBC)
  - Modeling of input and output ports for waveguide simulations
  - Comparisons with ABC and PML

Brief history of the development of DGTD methods

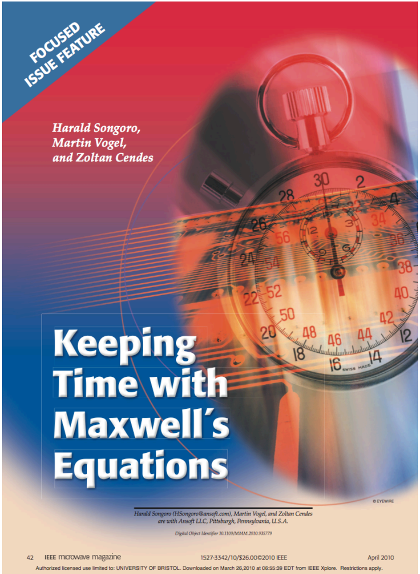
FOCUSED ISSUE FEATURE

Harald Songoro,
Martin Vogel,
and Zoltan Cendes

Keeping Time with Maxwell's Equations

© EYEWIRE

Harald Songoro (HSongoro@ansoft.com), Martin Vogel, and Zoltan Cendes are with Ansoft LLC, Pittsburgh, Pennsylvania, U.S.A.

Digital Object Identifier 10.1109/MMM.2010.935779

42 IEEE microwave magazine 1527-3342/10/$26.00©2010 IEEE April 2010

Authorized licensed use limited to: UNIVERSITY OF BRISTOL. Downloaded on March 26,2010 at 06:55:39 EDT from IEEE Xplore. Restrictions apply.

Introducing a commercial FETD solver breaks new ground in EM field simulation. Based on the DGTD method, it allows unstructured geometry-conforming meshes to be used for the first time in transient EM field simulation.

DGTD is a competitive alternative to traditional FDTD based methods to solving Maxwell's equations in the time domain. The applications presented here include the electromagnetic pulse susceptibility of the differential lines in a laptop computer, the radar signature of a landmine under undulating ground, the TDR of a bent flex circuit, and the return loss of a connector. All of these examples involve complicated, curved geometries where the flexibility of the unstructured meshes used in DGTD provides powerful advantages over simulation by conventional brick-shaped FDTD and FIT meshes.

IEEE Microwave Magazine - April 2010

- Higher order leap-frog time schemes

  H. Fahs and S. Lanteri
  J. Comput. Appl. Math., Vol. 234, 2010

- Locally implicit time schemes

  V. Dolean, H. Fahs, L. Fezoui and S. Lanteri
  J. Comput. Phys., Vol. 229, No. 2, 2010

  L. Moya, S. Descombes and S. Lanteri
  J. Sci. Comp., Vol. 56, No. 1, 2013

- Non-conforming triangular meshes

  H. Fahs
  Numer. Math. Theor. Meth. Appl., Vol. 2, No. 3, 2009

- Hybrid structured/unstructured meshes

  C. Durochat, S. Lanteri and C. Scheid
  Appl. Math. Comput., Vol. 224, 2013

  C. Durochat, S. Lanteri and R. Léger
  Int. J. Numer. Model., Electron. Netw. Devices Fields, Vol. 27, No. 3, 2014

Brief history of the development of DGTD methods

Our contributions (Januray 2007 to December 2013)

Numerical dosimetry - Collaboration with Orange Labs, Paris (2003 - 2011)

- H. Fahs, A. Hadjem, S. Lanteri, J. Wiart and M.F. Wong
  IEEE Trans. Ant. Propag., Vol. 59, No. 12, 2011
- DGTD method for time-domain Maxwell-Debye equations
- Software: GERShWIN
  (discontinuous GalERkin Solver for microWave INteraction with biological tissues)

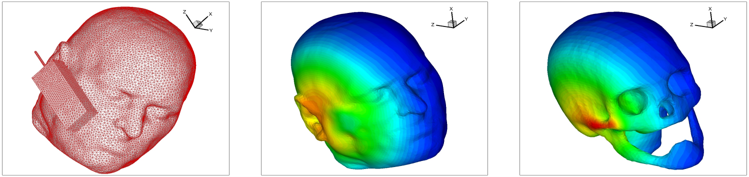

Exposure of head tissues to an electromagnetic wave emitted by a localized source. Contour lines of the amplitude of the electric field.

DEEP-ER FP7 EU project (October 2013 to March 2017)) (Dynamic Exascale Entry Platform - Extended Reach)

- Cluster-Booster architecture
- Hybrid MPI/OpenMP parallelization

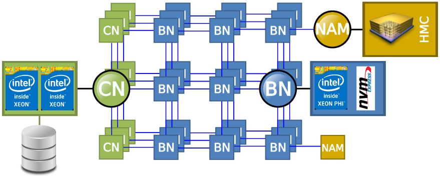

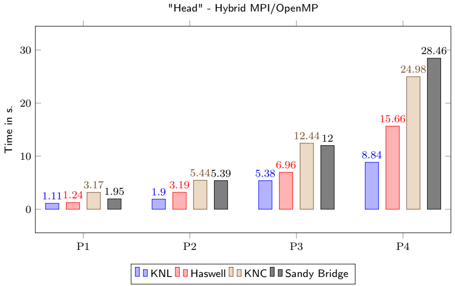

Hybrid MPI/OpenMP parallelization of the GERShWIN DGTD solver. Performance comparison between Intel Sandy Bridge nodes with 16 cores and Intel Haswell nodes with 24 cores, and Intel KNC and KNL nodes. Timings are given for the fastest combination of processes and threads we found for each case.

DEEP-ER FP7 EU project (October 2013 to March 2017)) (Dynamic Exascale Entry Platform - Extended Reach)

- Cluster-Booster architecture
- Hybrid MPI/OpenMP parallelization

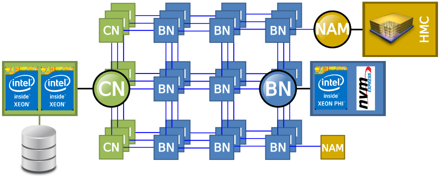

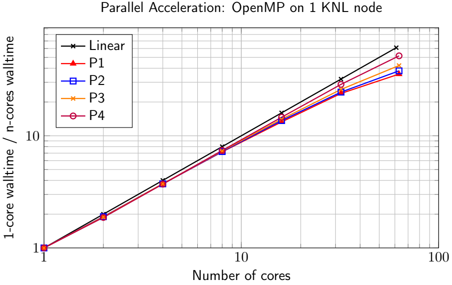

OpenMP parallelization of the GERShWIN DGTD solver
Strong scalability on a single Intel KNL node

- Nanophotonics is considered as a branch of optical engineering that deals with optics, or the interaction of light with particles or substances, at deeply subwavelength length scales
- Refers to phenomena of ultraviolet, visible and near IR light, with a wavelength of approximately 300 to 1200 nanometers
- Physical phenomena are characterized by a confinement of the electromagnetic field to the surface or tip of nanostructures resulting in a region referred to as the optical near field
- Starting-point PDE model: the system of Maxwell equations
  - Medium heterogeneity, geometrical features
  - Strong variations in spatial (and temporal) scales
  - Local, non-local and possibly non-linear dispersion effects

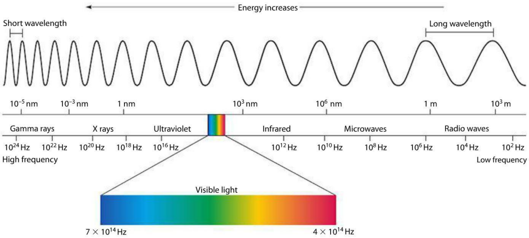

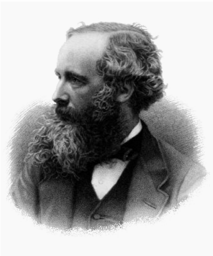

James Clerk Maxwell (1831-1879)

DGTD methods for nanophotonics

- Theoretical Optics and Photonics group, Humboldt-Universität zu Berlin
  - K. Busch, M. König and J. Niegemann
    Discontinuous Galerkin methods in nanophotonics
    Laser and Photonics Reviews, Vol. 5, No. 6, 2011
  - M. König, K. Busch and J. Niegemann
    The discontinuous Galerkin time-domain method for Maxwell's equations with anisotropic materials
    Photonics and Nanostructures - Fundamentals and Applications, Vol. 8, 2010
- Theoretical Electrical Engineering Group in Paderborn University
  - Y. Grynko, J. Förstner and T. Meier
    Application of the discontinous Galerkin time domain method to the optics of metallic nanostructures
    AAPP | Physical, Mathematical, and Natural Sciences, Vol. 89 (S1), 2011
- TU Dresden, Institut für Angewandte Photophysik
  - A. Hille, R. Kullock, S. Grafström and L. M. Eng
    Improving nano-optical simulations through curved elements implemented within the discontinuous Galerkin method
    J. Comput. Theor. Nanos., Vol. 7, 2010
- Increasingly studied in the recent years

The time-domain Maxwell-Drude equations

$$\varepsilon_{\text{local}}(\omega) = \varepsilon_r(\omega) = \varepsilon_\infty - \frac{\omega_d^2}{\omega^2 + i\omega\gamma_d}$$

$$\left\{ \begin{array}{rcl} \dfrac{\partial \mathbf{H}}{\partial t} & = & -\nabla \times \mathbf{E} \\ \dfrac{\partial \mathbf{E}}{\partial t} & = & \nabla \times \mathbf{H} - \mathbf{J}_p \\ \dfrac{\partial \mathbf{J}_p}{\partial t} + \gamma_d \mathbf{J}_p & = & \omega_d^2 \mathbf{E} \end{array} \right.$$

- Theoretical and numerical study
  - Analysis of a Generalized Dispersion Model (GDM)
    Development based on one 0th-order pole (ZOP), a set of 1st-order generalized poles (FOGP) and a set of 2nd-order generalized poles (SOGP)
  - Upwind flux DGTD method with LSRK time scheme
  - S. Lanteri, C. Scheid and J. Viquerat
    SIAM J. Sci. Comput., Vol. 39, No. 3, 2017

The time-domain Maxwell-GDM equations

$$\varepsilon_{r,g}(\omega) = \varepsilon_\infty - \frac{\sigma}{i\omega} - \sum_{l\in L_1} \frac{a_l}{i\omega - b_l} - \sum_{l\in L_2} \frac{c_l - i\omega d_l}{\omega^2 - e_l + i\omega f_l}$$

$$\left\{\begin{array}{rcll}
\dfrac{\partial \mathbf{H}}{\partial t} & = & -\nabla \times \mathbf{E} & \\
\varepsilon_\infty \dfrac{\partial \mathbf{E}}{\partial t} & = & \nabla \times \mathbf{H} - \mathbf{J}_0 - \displaystyle\sum_{l\in L_1} \mathbf{J}_l - \sum_{l\in L_2} \mathbf{J}_l, & \\
\mathbf{J}_0 & = & (\sigma + \displaystyle\sum_{l\in L_2} d_l)\mathbf{E}, & \\
\mathbf{J}_l & = & a_l \mathbf{E} - b_l \mathbf{P}_l & \forall l \in L_1, \\
\dfrac{\partial \mathbf{P}_l}{\partial t} & = & \mathbf{J}_l & \forall l \in L_1, \\
\dfrac{\partial \mathbf{J}_l}{\partial t} & = & (c_l - d_l f_l)\mathbf{E} - f_l \mathbf{J}_l - e_l \mathbf{P}_l & \forall l \in L_2, \\
\dfrac{\partial \mathbf{P}_l}{\partial t} & = & d_l \mathbf{E} + \mathbf{J}_l & \forall l \in L_2.
\end{array}\right.$$

Development of a dedicated software suite for nanophotonics

DIOGENeS - DIscOntinuous GalErkin Nano Solvers
https://diogenes.inria.fr

- 3D time-domain and frequency-domain Maxwell equations
- Drude, Drude-Lorentz and generalized dispersion models
- Silver-Muller absorbing boundary condition or CFS-PML technique
- TF/SF formulation for imposing complex source models
- High order polynomial interpolation
- Unstructured and hybrid cubic/tetrahedral meshes
- Affine and curvilinear elements
- Leap-frog (2nd and 4th order) and optimized Runge-Kutta time schemes
- Hybrid MIMD/SIMD parallelization based on MPI/OpenMP

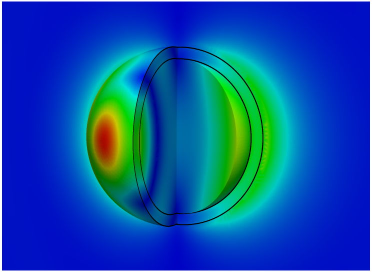

(d) Modulus of the **E** field in the vicinity of the nanoshell. A 4SOGP dispersion model is used to describe the gold shell

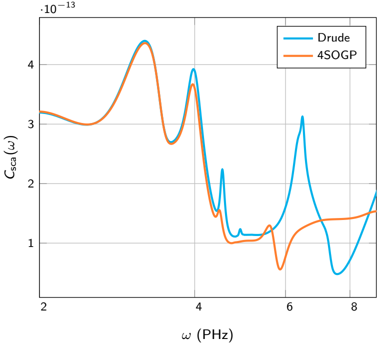

(e) Computed scattering cross-sections of the nanoshell for various gold dispersion models

Near-field solution and scattering cross-section of a silica/gold nanoshell device. $\mathbb{P}_4$ polynomial approximation is used for the spatial DG discretization, along with curvilinear element for an enhanced geometrical description of the shell.

DGTD method on curvilinear tetrahedral meshes

- Classical FEM rely on tessellations composed of straight-edged elements mapped linearly from a reference element
- This represents a serious hindrance for high order methods
- Exploit high order mappings for curvilinear tetrahedral elements

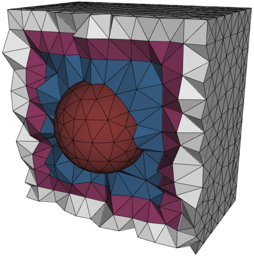

Tetrahedral mesh for plasmonic resonance of a gold nanosphere with radius 50 nm. The scatterer (in red) is enclosed by the total field (TF) region (in blue), delimited by the TF/SF interface on which the incident field is imposed. Then we find the scattered field (SF) region (in purple), surrounded by UPMLs (in gray).

DGTD method on curvilinear tetrahedral meshes

- Classical FEM rely on tessellations composed of straight-edged elements mapped linearly from a reference element
- This represents a serious hindrance for high order methods
- Exploit high order mappings for curvilinear tetrahedral elements

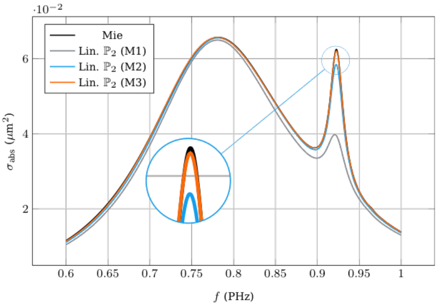

Mesh with affine elements

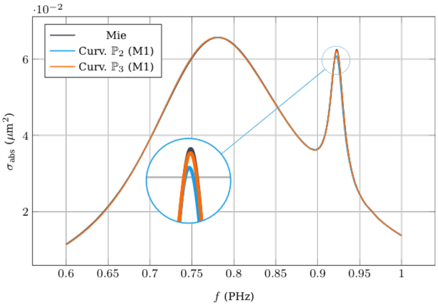

Mesh with curvilinear elements

Scattering cross section of a gold nanosphere obtained with P2 and P3 interpolation of the EM filed compenents, using affine (linear) and curvilinear meshes with various refinement levels.

DGTD method on curvilinear tetrahedral meshes

- Plasmonic coupling between nanoparticles is at the heart of many applications in nano-optics
- The coupled plasmon resonance induces very intense fields in the gap between the particles
- A proper near-field resolution is essential to a good understanding of the properties of such coupled structures

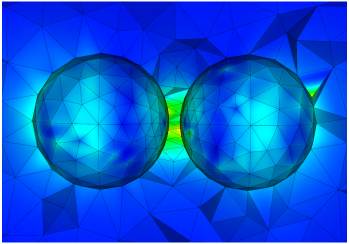

Mesh with affine elements

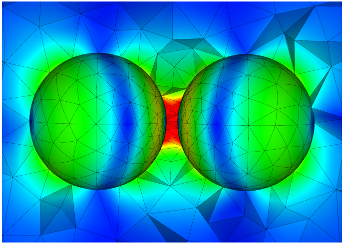

Mesh with curvilinear elements

Near-field visualization of the electric field Fourier transform for a gold nanosphere dimer. Surface-to-surface distance is set to 4 nm. Calculations are based on a DGTD-$\mathbb{P}_4$ method.

DGTD method on curvilinear tetrahedral meshes

- Plasmonic coupling between nanoparticles is at the heart of many applications in nano-optics
- The coupled plasmon resonance induces very intense fields in the gap between the particles
- A proper near-field resolution is essential to a good understanding of the properties of such coupled structures

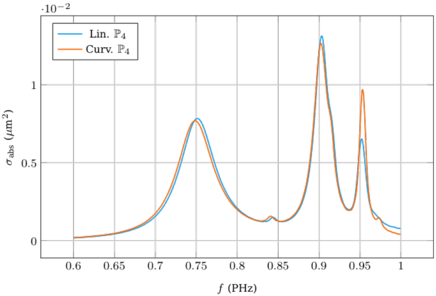

Absorption cross section of a gold nanosphere dimer obtained with P4 approximation using affine and curvilinear meshes. Calculations are based on a DGTD-$\mathbb{P}_4$ method.

DGTD with non-uniform distribution of the interpolation order

- Dealing with meshes showing large variations in cell size
- Impose low orders in small cells and high orders in large cells
- Time step-based distribution strategy

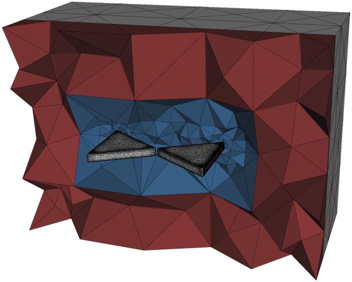

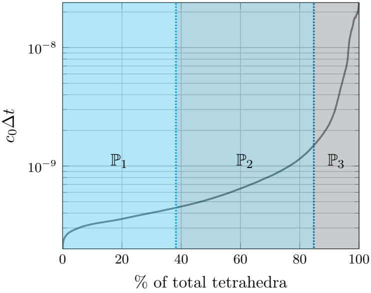

Computation of the extinction cross section of a metallic bowtie nanoantenna. Polynomial order repartition for the bowtie mesh with respect to time-step.

DGTD with non-uniform distribution of the interpolation order

- Dealing with meshes showing large variations in cell size
- Impose low orders in small cells and high orders in large cells
- Time step-based distribution strategy

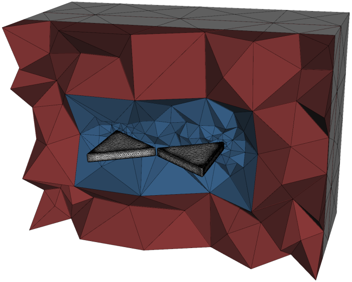

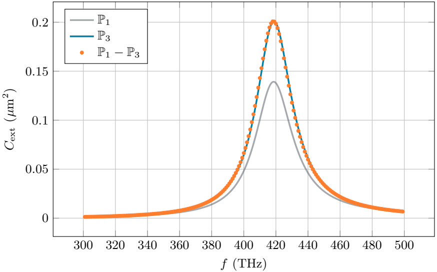

Extinction cross section of the bowtie nanoantenna obtained with $\mathbb{P}_1$, $\mathbb{P}_3$ and $\mathbb{P}_1 - \mathbb{P}_3$ approximations. Less than 2 % of relative error is observed between full $\mathbb{P}_3$ and $\mathbb{P}_1 - \mathbb{P}_3$ computations, for a speedup factor superior to 2.

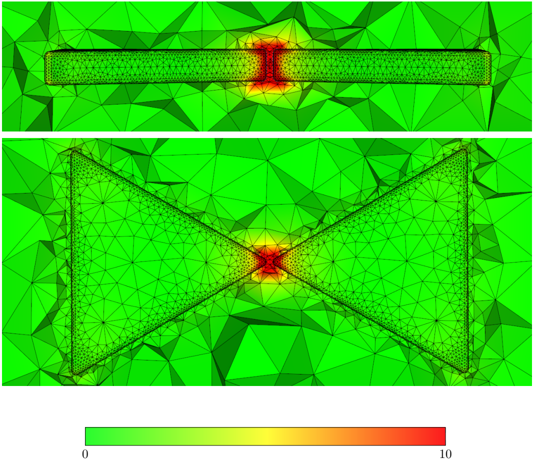

$|\mathbf{E}|$ field map in the bowtie antenna obtained with a $\mathbb{P}_1 - \mathbb{P}_3$ approximation. The field values are scaled to $[0, 10]$.

Application to photovoltaics
Light trapping in complex solar cell structures

- Realistic modeling of geometrical features such as textures
- Assessment of plasmomic effects on absorption
- For the design and optimization of solar cell structures
- In collaboration with Urs Aeberhard, IEK-5 Photovoltaik, Forschungszentrum Jülich, Germany

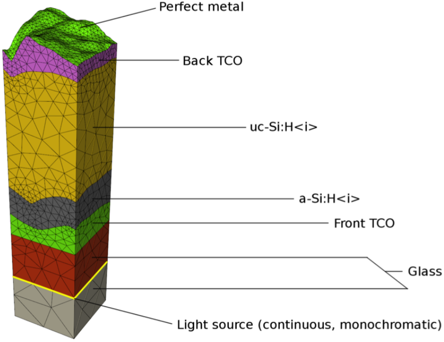

Application to photovoltaics
Light trapping in complex solar cell structures

- Starting from AFM (Atomic Force Microscopy) images
- Exploit MeshGems suite (http://www.meshgems.com/)
- Imposing periodicity

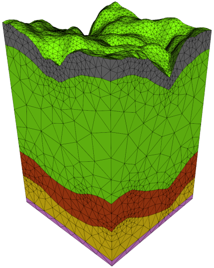

Original model

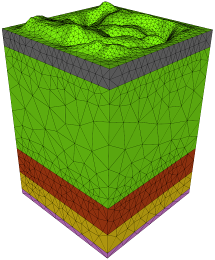

Modified model
with periodic boundaries

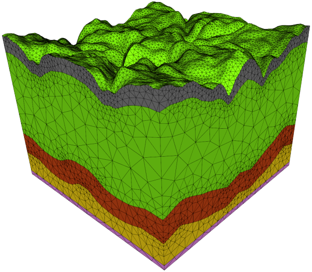

Symmetrized model

Application to photovoltaics - Light trapping in complex solar cell structures

- Dealing with optical data
  - Optical data are given from measurements and fitted to a generalized dispersion model
  - Sum of one 0th-order pole (ZOP), 1st-order generalized poles (FOGP), and 2nd-order generalized poles (SOGP)

$$\varepsilon_{r,g}(\omega) = \varepsilon_\infty - \frac{\sigma}{i\omega} - \sum_{l\in L_1} \frac{a_l}{i\omega - b_l} - \sum_{l\in L_2} \frac{c_l - i\omega d_l}{\omega^2 - e_l + i\omega f_l}$$

  - Optimization method based on Simulated Annealing

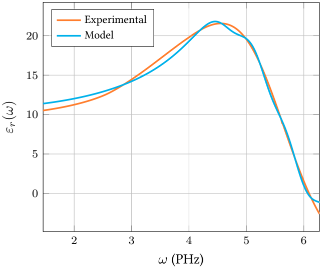

(f) Asi-i, real part.

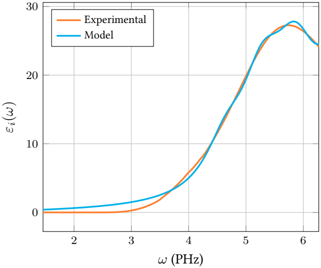

(g) Asi-i, imaginary part.

Application to photovoltaics
Light trapping in complex solar cell structures

- Performance results: Occigen Bull/Atos cluster at CINES
  Intel E5-2690, 2.6 GHz, 24 cores on each node, 64 GB or 128 GB RAM per node

Solver	# cores	Elapsed	Speedup
DGTD-$\mathbb{P}_1$	96	584 sec	1.00 (1.0)
-	192	292 sec	2.00 (2.0)
-	384	146 sec	4.00 (4.0)
DGTD-$\mathbb{P}_2$	96	974 sec	1.00 (1.0)
-	192	490 sec	2.00 (2.0)
-	384	246 sec	3.95 (4.0)
DGTD-$\mathbb{P}_3$	192	808 sec	1.00 (1.0)
-	384	418 sec	1.95 (2.0)

Strong scalability analysis of the DGTD-$\mathbb{P}_k$ solver on the Occigen system. Tetrahedral mesh with 305,265 vertices and 1,689,764 elements. Timings for 1000 time steps. Execution mode: 1 MPI process per core.

Hydrodynamic Drude model

- The existence of plasmons roots in the interaction between the free electrons of a metal with an external varying electromagnetic field
- Various models exist for modeling this coupling depending on the considered material and frequency range
- The most famous is the Drude model describing permittivity function of noble metals up to the visible range of frequencies
- All these models share a common assumption, which is the local response assumption (LRA)
- This hypothesis states that, at any point of the metal, the polarization of the electrons only depends on the electromagnetic fields at this precise point
- For scales approaching the nanometer, plasmons exhibit features that cannot be correctly predicted in the LRA framework
- Modified models are required, called non-local models (NLM), owing to their accounting for what happens in the vicinity of the electron to determine its response

The time-domain Maxwell-Hydrodynamic Drude equations

$$\varepsilon_r(\mathbf{k},\omega) = \varepsilon_\infty - \varepsilon_{\text{local}}(\omega) - \varepsilon_{\text{non local}}(\mathbf{k},\omega)$$

$$\left\{\begin{array}{rcl}
\dfrac{\partial \mathbf{H}}{\partial t} & = & -\nabla \times \mathbf{E} \\
\varepsilon_\infty \dfrac{\partial \mathbf{E}}{\partial t} & = & \nabla \times \mathbf{H} - \mathbf{J}_l - \mathbf{J}_{nl} \\
\dfrac{\partial \mathbf{J}_l}{\partial t} + \gamma_l \mathbf{J}_l & = & \omega_l^2 \mathbf{E} \\
\dfrac{\partial \mathbf{J}_{nl}}{\partial t} + \gamma_{nl} \mathbf{J}_{nl} & = & \beta^2 \nabla Q_{nl} + \omega_{nl}^2 \mathbf{E} \\
\dfrac{\partial Q_{nl}}{\partial t} & = & \nabla . \mathbf{J}_{nl}
\end{array}\right.$$

A. Moreau, C. Ciraci and D.R. Smith - Physical Review B 87, 045401 (2013)

S. Raza, S.I. Bozhevolnyi, M. Wubs, N.A. Mortensen
J. Phys.: Condens. Matter 27, 183204 (topical review, 2015)

The time-domain Maxwell-Hydrodynamic Drude equations

- Numerical study in the 2D case
  - Centered flux DGTD method with leap-frog time scheme
  - N. Schmitt, C. Scheid, S. Lanteri, A. Moreau and J. Viquerat
    J. Comput. Phys., Vol. 316, 2016

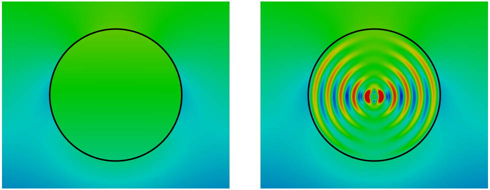

Local model　　　Non-local model

Non-local resonance of a gold nanodisk with radius 2 nm. The plots show the modulus of the electric field in the Fourier space. The right panel shows the excited bulk plasmon due to non-local model, which does not appear for the local model, on the left panel.

The time-domain Maxwell-Hydrodynamic Drude equations

- Extension to the 3D case
  - PhD thesis of Nikolai Schmitt, ongoing
  - Upwind flux, low storage Runge-Kutta and curvilinear elements
  - Preliminary results at PIERS 2017, St Petersburg, Russia, May 22-25

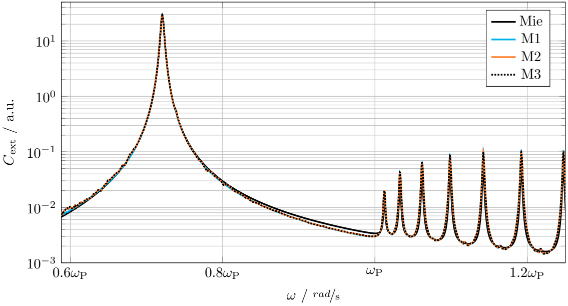

Scattering cross-section as a function of the frequency

Outline

1. Context
2. Time-domain modeling
   - Brief history of the development of DGTD methods
   - DGTD methods for nanoscale light/matter interactions
3. Frequency-domain modeling
   - Hybridizable DG method
   - Scalable DD-based HDG solver
4. Closure

The challenge with DG for frenquency-domain problems

3D frequency-domain Maxwell's equations

$$\begin{cases} \mathbf{i}\omega\varepsilon_r\mathbf{E} - \mathbf{curl}\,\mathbf{H} = -\mathbf{J}, \text{ in } \Omega \\ \mathbf{i}\omega\mu_r\mathbf{H} + \mathbf{curl}\,\mathbf{E} = 0, \text{ in } \Omega \\ \mathbf{n}\times\mathbf{E} = 0, \text{ on } \Gamma_m \\ \mathbf{n}\times\mathbf{E} + \mathbf{n}\times(\mathbf{n}\times\mathbf{H}) = \mathbf{n}\times\mathbf{E}^{\mathrm{inc}} + \mathbf{n}\times(\mathbf{n}\times\mathbf{H}^{\mathrm{inc}}), \text{ on } \Gamma_a \end{cases}$$

Classical DG formulation

- Naturally adapted to heterogeneous media and discontinuous solutions
- Can easily deal with unstructured, possibly non-conforming meshes (h-adaptivity)
- High order with compact stencils and non-conforming approximations (p-adaptivity)
- Usually rely on polynomial interpolation but can also accomodate alternative functions (e.g plane waves)
- Amenable to efficient parallelization
- But leads to larger problems compared to continuous finite element methods

- B. Cockburn, J. Gopalakrishnan and R. Lazarov
  Unified hybridization of discontinuous Galerkin, mixed, and continuous Galerkin methods for second order elliptic problems
  SIAM J. Numer. Anal., Vol. 47, No. 2 (2009)

- N.C. Nguyen, J. Peraire and B. Cockburn
  Hybridizable discontinuous Galerkin methods for the time-harmonic Maxwell's equations
  J. Comput. Phys., Vol. 230, No. 19 (2011)

- S. Lanteri, L. Li and R. Perrussel
  Numerical investigation of a high order hybridizable discontinuous Galerkin method for 2d time-harmonic Maxwell's equations
  COMPEL, Vol. 2, No. 3, pp. 1112-1138 (2013)

- L. Li, S. Lanteri and R. Perrussel
  A hybridizable discontinuous Galerkin method combined to a Schwarz algorithm for the solution of 3d time-harmonic Maxwell's equation
  J. Comput. Phys., Vol. 256, pp. 563-581 (2014)

Hybridizable DG method in 3D

Principles of a HDG formulation

- Keep the advantages of classical DG methods
- Introduce an hybrid variable to decouple local problems defined at the element level
- Solve a reduced linear system for the hybrid variable unknowns only

Complexity: number of globally coupled degrees of freedom

- Classical DG method with $\mathbb{P}_p$ interpolation

$$(p+1)(p+2)(p+3)N_e \quad , \quad N_e \text{ is the } \# \text{ of elements}$$

- HDG method with $\mathbb{P}_p$ interpolation

$$(p+1)(p+2)N_f \quad , \quad N_f \text{ is the } \# \text{ of faces}$$

- For a simplicial mesh $N_f \approx 2N_e$ and the ratio DG/HDG is $\approx \dfrac{p+3}{2}$
- Continuous finite element formulation based on Nedelec's first family of face/edge elements in a simplex (tetrahedron)

$$\frac{p(p+2)(p+3)}{2} N_e$$

- For a simplicial mesh $N_f \approx 2N_e$ and the ratio HDG/FE is $\approx \dfrac{4(p+1)}{p(p+3)}$

Principles of a HDG formulation

- Keep the advantages of classical DG methods
- Introduce an hybrid variable to decouple local problems defined at the element level
- Solve a reduced linear system for the hybrid variable unknowns only

Complexity: number of globally coupled degrees of freedom

- Classical DG method with $\mathbb{P}_p$ interpolation

$$(p+1)(p+2)(p+3)N_e \quad , \quad N_e \text{ is the \# of elements}$$

- HDG method with $\mathbb{P}_p$ interpolation

$$(p+1)(p+2)N_f \quad , \quad N_f \text{ is the \# of faces}$$

- For a simplicial mesh $N_f \approx 2N_e$ and the ratio DG/HDG is $\approx \dfrac{p+3}{2}$
- Continuous finite element formulation based on Nedelec's first family of face/edge elements in a simplex (tetrahedron)

$$\frac{p(p+2)(p+3)}{2}N_e$$

- For a simplicial mesh $N_f \approx 2N_e$ and the ratio HDG/FE is $\approx \dfrac{4(p+1)}{p(p+3)}$

Notations and definitions

- $\mathcal{T}_h$ a simplicial mesh of the computational domain
- $\mathcal{F}_h^I$ and $\mathcal{F}_h^B$ the union of all inner and boundary faces of $\mathcal{T}_h$, respectively ($\mathcal{F}_h := \mathcal{F}_h^I \cup \mathcal{F}_h^B$)
- Discontinuous FE spaces

$$\mathbf{V}_h = \left\{ \mathbf{v}^* \in \left[L^2(\Omega) \right]^3 \mid \mathbf{v}^*|_{K_e} \in [\mathbb{P}_{p_e}(K_e)]^3, \quad \forall K_e \in \mathcal{T}_h \right\}$$

$$\mathbf{M}_h = \left\{ \boldsymbol{\eta} \in \left[L^2(\mathcal{F}_h) \right]^3 \mid \boldsymbol{\eta}|_{F_f} \in [\mathbb{P}_{p_f}(F_f)]^3, (\boldsymbol{\eta} \cdot \mathbf{n})\,|_{F_f} = 0, \quad \forall F_f \in \mathcal{F}_h \right\}$$

- For a face $F = \overline{K}^+ \cap \overline{K}^-$, we define *mean* (*average*) *values* $\{\cdot\}$ and *jumps* $[\![\cdot]\!]$, $[\![[\![\cdot]\!]]\!]$

$$\{\mathbf{v}\}_F = \frac{1}{2}(\mathbf{v}^+ + \mathbf{v}^-) \ , \ [\![\mathbf{v}]\!]_F = \mathbf{n}^+ \times \mathbf{v}^+ + \mathbf{n}^- \times \mathbf{v}^- \quad \text{and} \quad [\![[\![\mathbf{v}]\!]]\!]_F = \mathbf{v}^+ - \mathbf{v}^-$$

where $\mathbf{n}^\pm$ the outward unitary normals, $\mathbf{v}^\pm$ the traces of $\mathbf{v}$ on F.

Local formulation

Find $(\mathbf{E}_h, \mathbf{H}_h)$ in the space $\mathbf{V}_h \times \mathbf{V}_h$ such that (for all K in $\mathcal{T}_h$)

$$\begin{cases} (\mathbf{i}\omega\varepsilon\mathbf{E}_h, \mathbf{v}^*)_K - (\mathbf{H}_h, \mathbf{curl}\,\mathbf{v}^*)_K + \left\langle \gamma_{\mathrm{t}}(\hat{\mathbf{H}}_h), \mathbf{n}\times\mathbf{v}^* \right\rangle_{\partial K} = 0, \;\; \forall \mathbf{v}^* \in \mathbf{V}_h, \\ (\mathbf{i}\omega\mu\mathbf{H}_h, \mathbf{v}^*)_K + (\mathbf{E}_h, \mathbf{curl}\,\mathbf{v}^*)_K - \left\langle \gamma_{\mathrm{t}}(\hat{\mathbf{E}}_h), \mathbf{n}\times\mathbf{v}^* \right\rangle_{\partial K} = 0, \;\; \forall \mathbf{v}^* \in \mathbf{V}_h. \end{cases}$$

with $\gamma_{\mathrm{t}}(\cdot) = -\mathbf{n}\times(\mathbf{n}\times\cdot)$.

Numerical traces

$$\begin{cases} \boldsymbol{\Lambda}_h := \gamma_{\mathrm{t}}(\hat{\mathbf{H}}_h), \quad \forall F \in \mathcal{F}_h \\ \gamma_{\mathrm{t}}(\hat{\mathbf{E}}_h) = \gamma_{\mathrm{t}}(\mathbf{E}_h) + \tau^K \mathbf{n}\times(\boldsymbol{\Lambda}_h - \gamma_{\mathrm{t}}(\mathbf{H}_h)), \quad \text{on } \partial K \end{cases}$$

where τ is a stabilization parameter.

Global formulation of the HDG method

Find $(\mathbf{E}_h, \mathbf{H}_h, \mathbf{\Lambda}_h) \in \mathbf{V}_h \times \mathbf{V}_h \times \mathbf{M}_h$ such that $\forall (\mathbf{v}^*, \mathbf{\Lambda}^*) \in \mathbf{V}_h \times \mathbf{M}_h$

$$\left\{\begin{aligned} (\mathbf{i}\omega\varepsilon\mathbf{E}_h, \mathbf{v}^*)_{\mathcal{T}_h} - (\mathbf{H}_h, \mathbf{curl}\,\mathbf{v}^*)_{\mathcal{T}_h} + \langle \mathbf{\Lambda}_h, \mathbf{n}\times\mathbf{v}^*\rangle_{\partial\mathcal{T}_h} &= 0 \\ (\mathbf{i}\omega\mu\mathbf{H}_h, \mathbf{v}^*)_{\mathcal{T}_h} + (\mathbf{E}_h, \mathbf{curl}\,\mathbf{v}^*)_{\mathcal{T}_h} - \left\langle \gamma_{\mathrm{t}}(\hat{\mathbf{E}}_h), \mathbf{n}\times\mathbf{v}^*\right\rangle_{\partial\mathcal{T}_h} &= 0 \\ \left\langle [\![\gamma_{\mathrm{t}}(\hat{\mathbf{E}}_h)]\!], \mathbf{\Lambda}^*\right\rangle_{\mathcal{F}_h} - \langle \mathbf{\Lambda}_h, \mathbf{\Lambda}^*\rangle_{\Gamma_a} - &= \left\langle \mathbf{g}^{\mathrm{inc}}, \mathbf{\Lambda}^*\right\rangle_{\Gamma_a} \end{aligned}\right.$$

Using the definition of the numerical traces

$$\left\{\begin{aligned} (\mathbf{i}\omega\varepsilon\mathbf{E}_h, \mathbf{v}^*)_{\mathcal{T}_h} - (\mathbf{H}_h, \mathbf{curl}\,\mathbf{v}^*)_{\mathcal{T}_h} + \langle \mathbf{\Lambda}_h, \mathbf{n}\times\mathbf{v}^*\rangle_{\partial\mathcal{T}_h} &= 0 \\ (\mathbf{i}\omega\mu\mathbf{H}_h, \mathbf{v}^*)_{\mathcal{T}_h} + (\mathbf{curl}\,\mathbf{E}_h, \mathbf{v}^*)_{\mathcal{T}_h} + \langle \tau\mathbf{n}\times(\mathbf{H}_h - \mathbf{\Lambda}_h), \mathbf{n}\times\mathbf{v}^*\rangle_{\partial\mathcal{T}_h} &= 0 \\ \langle \mathbf{n}\times\mathbf{E}_h, \mathbf{\Lambda}^*\rangle_{\partial\mathcal{T}_h} + \langle \tau(\gamma_{\mathrm{t}}(\mathbf{H}_h) - \mathbf{\Lambda}_h), \mathbf{\Lambda}^*\rangle_{\partial\mathcal{T}_h} - \langle \mathbf{\Lambda}_h, \mathbf{\Lambda}^*\rangle_{\Gamma_a} &= \left\langle \mathbf{g}^{\mathrm{inc}}, \mathbf{\Lambda}^*\right\rangle_{\Gamma_a} \end{aligned}\right.$$

Global formulation of the HDG method

Find $(\mathbf{E}_h, \mathbf{H}_h, \mathbf{\Lambda}_h) \in \mathbf{V}_h \times \mathbf{V}_h \times \mathbf{M}_h$ such that $\forall (\mathbf{v}^*, \mathbf{\Lambda}^*) \in \mathbf{V}_h \times \mathbf{M}_h$

$$\begin{cases} (\mathbf{i}\omega\varepsilon\mathbf{E}_h, \mathbf{v}^*)_{\mathcal{T}_h} - (\mathbf{H}_h, \mathbf{curl}\,\mathbf{v}^*)_{\mathcal{T}_h} + \langle \mathbf{\Lambda}_h, \mathbf{n} \times \mathbf{v}^* \rangle_{\partial\mathcal{T}_h} = 0 \\ (\mathbf{i}\omega\mu\mathbf{H}_h, \mathbf{v}^*)_{\mathcal{T}_h} + (\mathbf{E}_h, \mathbf{curl}\,\mathbf{v}^*)_{\mathcal{T}_h} - \left\langle \gamma_{\mathrm{t}}(\hat{\mathbf{E}}_h), \mathbf{n} \times \mathbf{v}^* \right\rangle_{\partial\mathcal{T}_h} = 0 \\ \left\langle [\![\gamma_{\mathrm{t}}(\hat{\mathbf{E}}_h)]\!], \mathbf{\Lambda}^* \right\rangle_{\mathcal{F}_h} - \langle \mathbf{\Lambda}_h, \mathbf{\Lambda}^* \rangle_{\Gamma_a} - = \left\langle \mathbf{g}^{\mathrm{inc}}, \mathbf{\Lambda}^* \right\rangle_{\Gamma_a} \end{cases}$$

Using the definition of the numerical traces

$$\begin{cases} (\mathbf{i}\omega\varepsilon\mathbf{E}_h, \mathbf{v}^*)_{\mathcal{T}_h} - (\mathbf{H}_h, \mathbf{curl}\,\mathbf{v}^*)_{\mathcal{T}_h} + \langle \mathbf{\Lambda}_h, \mathbf{n} \times \mathbf{v}^* \rangle_{\partial\mathcal{T}_h} = 0 \\ (\mathbf{i}\omega\mu\mathbf{H}_h, \mathbf{v}^*)_{\mathcal{T}_h} + (\mathbf{curl}\,\mathbf{E}_h, \mathbf{v}^*)_{\mathcal{T}_h} + \langle \tau\mathbf{n} \times (\mathbf{H}_h - \mathbf{\Lambda}_h), \mathbf{n} \times \mathbf{v}^* \rangle_{\partial\mathcal{T}_h} = 0 \\ \langle \mathbf{n} \times \mathbf{E}_h, \mathbf{\Lambda}^* \rangle_{\partial\mathcal{T}_h} + \langle \tau(\gamma_{\mathrm{t}}(\mathbf{H}_h) - \mathbf{\Lambda}_h), \mathbf{\Lambda}^* \rangle_{\partial\mathcal{T}_h} - \langle \mathbf{\Lambda}_h, \mathbf{\Lambda}^* \rangle_{\Gamma_a} = \left\langle \mathbf{g}^{\mathrm{inc}}, \mathbf{\Lambda}^* \right\rangle_{\Gamma_a} \end{cases}$$

Electromagnetic field

$\left(\mathbf{E}_h|_{K_e}, \mathbf{H}_h|_{K_e}\right) := \left(\mathbf{E}^e, \mathbf{H}^e\right)$

$\mathbf{E}^e(\mathbf{x}) = \left[E_x^e(\mathbf{x}), E_y^e(\mathbf{x}), E_z^e(\mathbf{x})\right]^T$ and $\mathbf{H}^e(\mathbf{x}) = \left[H_x^e(\mathbf{x}), H_y^e(\mathbf{x}), H_z^e(\mathbf{x})\right]^T$

We seek an approximation of the components of the EM field by a linear combination of basis functions $\varphi_j^e(\mathbf{x}) \in \mathbb{P}_{p_e}(K_e)$, *i.e.*

$$E_\xi^e(\mathbf{x}) = \sum_{j=1}^{N_K^e} \underline{E}_\xi^e[j]\,\varphi_j^e(\mathbf{x}), \quad H_\xi^e(\mathbf{x}) = \sum_{j=1}^{N_K^e} \underline{H}_\xi^e[j]\,\varphi_j^e(\mathbf{x})$$

where $\xi \in \{x, y, z\}$ and $\underline{E}_\xi^e[j]$, $\underline{H}_\xi^e[j]$ are the DoF.

Hybrid variable

$\mathbf{\Lambda}_h|_{F_f} := \mathbf{\Lambda}^f$ and $\mathbf{\Lambda}^f(\mathbf{x}) = \Lambda_{\mathbf{u}}^f(\mathbf{x})\,\mathbf{u}^f + \Lambda_{\mathbf{w}}^f(\mathbf{x})\,\mathbf{w}^f$

We seek an approximation of the components of the hybrid variable by a linear combination of basis functions $\psi_j^f(\mathbf{x})$ of $\mathbb{P}_{p_f}(F_f)$, *i.e.*

$$\text{where } \Lambda_{\boldsymbol{\nu}}^f(\mathbf{x}) = \sum_{j=1}^{N_F^f} \underline{\Lambda}_{\boldsymbol{\nu}}^f[j]\,\psi_j^f(\mathbf{x}) \quad \boldsymbol{\nu} \in \{\mathbf{u}, \mathbf{w}\} \text{ and } \underline{\Lambda}_{\boldsymbol{\nu}}^f[j] \text{ are the DoF.}$$

Global linear system for hybrid variable

$$\mathbb{K}\underline{\Lambda} = \underline{\mathbf{g}}$$

where

$$\mathbb{K} = \sum_{e=1}^{|\mathcal{T}_h|} [\mathcal{A}^e_{HDG}]^T \left(-\mathbb{B}^e [\mathbb{A}^e]^{-1} \mathbb{C}^e + \mathbb{G}^e\right) \mathcal{A}^e_{HDG}$$

and

$$\underline{\mathbf{g}} = \sum_{e=1}^{|\mathcal{T}_h|} \underline{\mathbf{g}}^e$$

$\mathcal{A}^e_{HDG}$ maps the DoF of the global trace on $\mathcal{F}_h$ to the DoF of the local trace on ∂K^e.

Local linear system for EM field

$$\mathbb{A}^e \underline{W}^e = -\mathbb{C}^e \mathcal{A}^e_{HDG} \underline{\Lambda}$$

where

$$\underline{W}^e = \left[\underline{E}^e_x, \underline{E}^e_y, \underline{E}^e_z, \underline{H}^e_x, \underline{H}^e_y, \underline{H}^e_z\right]^T$$

Hybridizable DG method in 3D

ANR TECSER project (May 2014 - April 2017)
Funded by DGA (French armament procurement agency)
http://www-sop.inria.fr/nachos/projects/tecser

- Implementation of HDG for arbitrary high order interpolation
- Local definition (element-wise and face-wise) of the interpolation degree
- Extension of the formulation to a non-conforming hybrid hexahedral/tetrahedral mesh
- Scalability improvement
  PDE-based Schwarz domain decomposition algorithm
  Algebraic domain decomposition algorithm (MaPHyS solver)
- Coupling with a BEM for an accurate treatement of far field radiation
- HORSE software
  High Order solver for Radar cross Section Evaluation

PDE-based domain decomposition approach: Schwarz algorithm

- Time-harmonic Maxwell equations in global vectorial form

$$\mathcal{L}\mathbf{W} = \mathbf{g} \quad \text{in } \Omega$$

- $\Omega = \bigcup_{j=1}^{N_s} \Omega_j$, $\mathbf{W}^j = \mathbf{W}|_{\Omega_j}$ with N_s : # subdomains

$$\begin{cases} \mathcal{L}\mathbf{W}^{j,p+1} & = & 0 \ \text{ in } \Omega_j \\ \mathcal{B}_{\mathbf{n}_{jl}}\mathbf{W}^{j,p+1} & = & \mathcal{B}_{\mathbf{n}_{jl}}\mathbf{W}^{l,p} \ \text{ on } \Gamma_{jl} = \partial\Omega_j \cap \bar{\Omega}_l \\ G_{\mathbf{n}}^{-}\mathbf{W}^{j,p+1} & = & G_{\mathbf{n}}^{-}\mathbf{W}_{\mathrm{inc}} \ \text{ on } \Omega_j \cap \Gamma_a \end{cases}$$

- Classical (natural) interface conditions: $\mathcal{B}_{\mathbf{n}} \equiv G_{\mathbf{n}}^{-}$

$$G_{\mathbf{n}}^{-}\mathbf{W} \iff \frac{1}{Z_r}(\mathbf{n}\times\mathbf{E}) + \mathbf{n}\times(\mathbf{n}\times\mathbf{H}) = \frac{1}{Z_r}(\mathbf{n}\times\mathbf{E}) - \gamma_{\mathrm{t}}(\mathbf{H}) \quad \text{(impedance condition)}$$

with $Z_r = \sqrt{\dfrac{\mu_r}{\varepsilon_r}}$

PDE-based domain decomposition approach: Schwarz algorithm

- L. Li, S. Lanteri and R. Perrussel
  A hybridizable discontinuous Galerkin method combined to a Schwarz algorithm for the solution of 3d time-harmonic Maxwell's equation
  J. Comput. Phys., Vol. 256, pp. 563- 581 (2014)
  - Conditions targeted by the HDG scheme on each interior face

$$[\![\hat{\mathbf{E}}_h]\!] = 0 \quad \text{and} \quad [\![[\![\mathbf{\Lambda}_h]\!]]\!] = 0$$

  with $\mathbf{n} \times \hat{\mathbf{E}}_h = \mathbf{n} \times \gamma_{\mathrm{t}}(\hat{\mathbf{E}}_h)$ and $\gamma_{\mathrm{t}}(\hat{\mathbf{E}}_h) = -\mathbf{n} \times (\mathbf{n} \times \hat{\mathbf{E}}_h)$.

  - In Ω_i, $\mathbf{\Lambda}_h^{(i)}$ is by definition single-valued on each face
    $\Rightarrow$ For any face in the interior of Ω_i, $[\![[\![\mathbf{\Lambda}_h^{(i)}]\!]]\!] = 0$ is automatically satisfied
  - At the interface between two subdomains Ω_i and Ω_j, the hybrid variables is *a priori* double-valued
    $\Rightarrow [\![[\![\mathbf{\Lambda}_h]\!]]\!] = \mathbf{\Lambda}_h^{(i)} - \mathbf{\Lambda}_h^{(j)} = 0$ has to be explicitly enforced
  - Equivalent condition

$$[\![\hat{\mathbf{E}}_h]\!] - Z_r^{(1)}[\![[\![\mathbf{\Lambda}_h]\!]]\!] = 0 \quad \text{and} \quad [\![\hat{\mathbf{E}}_h]\!] + Z_r^{(2)}[\![[\![\mathbf{\Lambda}_h]\!]]\!] = 0$$

Plane wave in vacuum

- Computational domain: the unit cube $\Omega = [0.0, 1.0]^3$
- Silver-Müller absorbing boundary condition on $\partial\Omega$
- Electromagnetic parameters: $\varepsilon = \ mu = 1$
- Fequency: 600 MHz
- Wavelength: $\lambda \simeq 0.5$ m
- Penalty parameter: $\tau = 1$

Mesh	# elements	# faces	h
M1	$2,692$	$5,544$	0.2500
M2	$6,144$	$12,928$	0.1875
M3	$12,000$	$25,000$	0.1500
M4	$20,736$	$42,912$	0.1250

Characteristics of regular tetrahedral meshes used for numerical convergence analysis

Plane wave in vacuum

- Computational domain: the unit cube $\Omega = [0.0, 1.0]^3$
- Silver-Müller absorbing boundary condition on $\partial\Omega$
- Electromagnetic parameters: $\varepsilon = \mu = 1$
- Fequency: 600 MHz
- Wavelength: $\lambda \simeq 0.5$ m
- Penalty parameter: $\tau = 1$

HDG method	# DoF for $\mathbf{\Lambda}$ field	# DoF for **EM** field
HDG-$\mathbb{P}_1$	257,472	497,664
HDG-$\mathbb{P}_2$	514,944	1,244,160
HDG-$\mathbb{P}_3$	858,240	2,488,320
HDG-$\mathbb{P}_4$	1,287,360	4,354,560

Discrete system size for mesh M4 (# elements = 20,736)

Plane wave in vacuum: numerical convergence analysis ($\text{Error} = \|\mathbf{E} - \mathbf{E}_h\|_2$)

	Error	Order
M1	7.10 e^{-02}	–
M2	4.27 e^{-02}	1.8
M3	2.85 e^{-02}	1.8
M4	2.03 e^{-02}	1.9

HDG-$\mathbb{P}_1$

	Error	Order
M1	6.78 e^{-03}	–
M2	2.90 e^{-03}	2.9
M3	1.49 e^{-03}	3.0
M4	8.68 e^{-04}	3.0

HDG-$\mathbb{P}_2$

	Error	Order
M1	3.89 e^{-04}	–
M2	1.24 e^{-04}	4.0
M3	5.09 e^{-05}	4.0
M4	2.46 e^{-05}	4.0

HDG-$\mathbb{P}_3$

	Error	Order
M1	2.05 e^{-05}	–
M2	4.89 e^{-06}	5.0
M3	1.61 e^{-06}	5.0
M4	6.48 e^{-07}	5.0

HDG-$\mathbb{P}_4$

$\Rightarrow$ Optimal convergence order (similar results for $\|\mathbf{H} - \mathbf{H}_h\|_2$)

Numerical dosimetry - SAR calculation

SAR measures the rate at which electric energy is absorbed by the tissues when exposed to an electromagnetic field

- Represents the power absorbed per mass of tissues and has units of W·kg^{-1}

$$\mathrm{SAR}(\mathbf{x}) = \sigma(\mathbf{x})\,|\mathbf{E}(\mathbf{x})|^2\,/\,\rho(\mathbf{x})$$

  - σ electric conductivity (S·m^{-1})
  - $\mathbf{E}$ electric field (V·m^{-1})
  - ρ density (Kg·m^{-3})

Numerical dosimetry - SAR calculation
Exposure of head tissues to a localized source

- Computational domain
  - Artificial boundary: sphere of radius $r = 0.3$ m
  - Heterogeneous geometrical model of the head tissues
- Source term: $\mathbf{J}_z = Z_0\delta(\mathbf{x} - \mathbf{x}^s)$
  - Z_0 free impedance
  - δ Dirac delta function
  - $\mathbf{x}^s = (-0.100, 0.025, -0.015)$: localization of the source
- Frequency: 1.8 GHz

	Vacuum	Skin	Skull	CSF	Brain
ε	1.00	38.66	11.60	68.25	43.88
σ (S·m^{-1})	0.00	1.18	0.27	2.28	0.97
λ (mm)	166.6	26.79	48.90	20.16	25.14
ρ	1.0	1100.0	1200.0	1000.0	1050.0

Numerical dosimetry - SAR calculation
Exposure of head tissues to a localized source

- Unstructured tetrahedral mesh: 1,853,832 elements and 3,911,256 faces
- Fequency: 1.8 GHz - Penalty parameter: $\tau = 1$

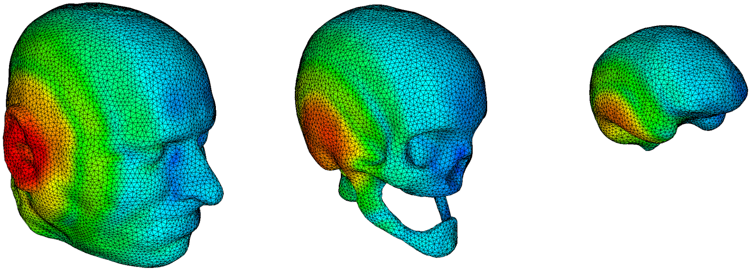

Contour lines of SAR - HDG$-\mathbb{P}_1$ method

Numerical dosimetry - SAR calculation
Exposure of head tissues to a localized source

- Unstructured tetrahedral mesh: 1,853,832 elements and 3,911,256 faces
- Fequency: 1.8 GHz - Penalty parameter: $\tau = 1$

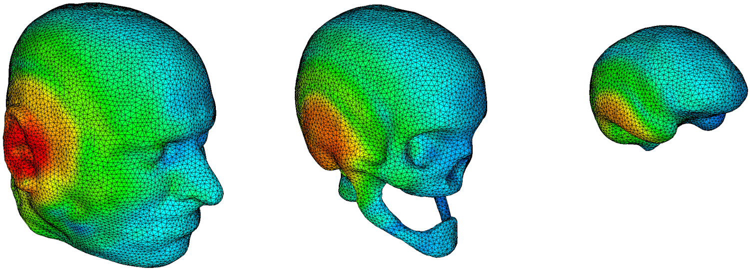

Contour lines of SAR - HDG$-\mathbb{P}_2$ method

Numerical dosimetry - SAR calculation
Exposure of head tissues to a localized source

- Unstructured tetrahedral mesh: 1,853,832 elements and 3,911,256 faces
- Fequency: 1.8 GHz - Penalty parameter: $\tau = 1$

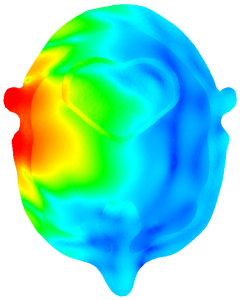

HDG$-\mathbb{P}_1$ method

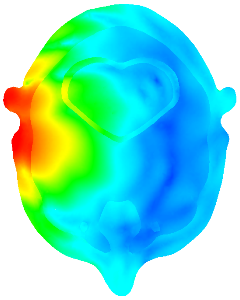

HDG$-\mathbb{P}_2$ method

Contour lines of SAR

Numerical dosimetry - SAR calculation
Exposure of head tissues to a localized source

- Unstructured tetrahedral mesh: 1,853,832 elements and 3,911,256 faces
- Fequency: 1.8 GHz - Penalty parameter: $\tau = 1$

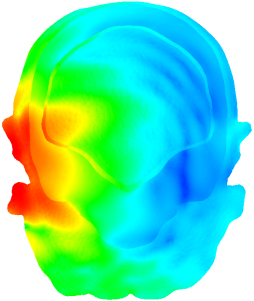

HDG$-\mathbb{P}_1$ method

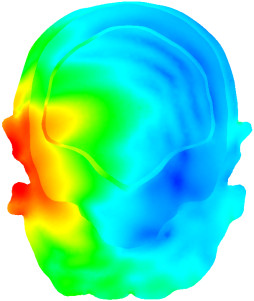

HDG$-\mathbb{P}_2$ method

Contour lines of SAR

Numerical dosimetry - SAR calculation
Exposure of head tissues to a localized source

- Unstructured tetrahedral mesh: 1,853,832 elements and 3,911,256 faces
- Fequency: 1.8 GHz - Penalty parameter: $\tau = 1$
- HDG$-\mathbb{P}_{ploc}$ method targeting 9 points per wavelength

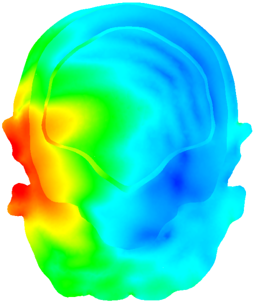

HDG$-\mathbb{P}_2$ method

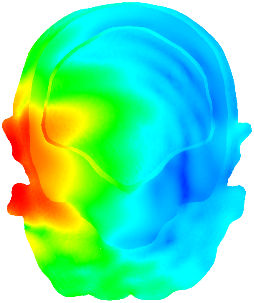

HDG$-\mathbb{P}_{ploc}$ method

Contour lines of SAR

Numerical dosimetry - SAR calculation
Exposure of head tissues to a localized source

- Unstructured tetrahedral mesh: 1,853,832 elements and 3,911,256 faces
- Fequency: 1.8 GHz - Penalty parameter: $\tau = 1$

# DoF **EM**: 49,312,008	**Λ**: 24,352,518
$\mathbb{P}_1$: 41,282,088	$\mathbb{P}_1$: 20,213,250
$\mathbb{P}_2$: 8,019,480	$\mathbb{P}_2$: 4,131,468
$\mathbb{P}_3$: 10,440	$\mathbb{P}_3$: 7,800
$\mathbb{P}_4$: 0	$\mathbb{P}_4$: 0

Distribution of the interpolation degree
in elements and faces of the mesh

Numerical dosimetry - SAR calculation
Exposure of head tissues to a localized source

- Unstructured tetrahedral mesh: 1,853,832 elements and 3,911,256 faces
- Fequency: 1.8 GHz - Penalty parameter: $\tau = 1$
- Performance results: Occigen Bull/Atos cluster at CINES
  Intel E5-2690, 2.6 GHz, 24 cores on each node, 64 GB or 128 GB RAM per node

HDG method	# cores	# iter	Fact. Time	Sol. Time	Wall time	Speedup
HDG-$\mathbb{P}_2$	384	52	21.1 sec	255.6 sec	278.4 sec	1.00
-	768	65	6.5 sec	142.4 sec	149.6 sec	1.85
-	1536	78	2.5 sec	79.2 sec	82.4 sec	3.40
HDG-$\mathbb{P}_{ploc}$	192	42	51.0 sec	288.1 sec	341.0 sec	1.00
	384	54	13.7 sec	159.6 sec	174.1 sec	1.95
-	768	60	4.5 sec	84.7 sec	89.6 sec	3.80
-	1536	74	1.6 sec	52.0 sec	53.9 sec	6.35

Strong scalability analysis: PDE-based Schwarz algorithm with PaStiX as a local solver

Scattering of a plane wave by a jet

- Unstructured tetrahedral mesh: 1,645,874 elements and 3,521,251 faces
- Fequency: 600 MHz - Wavelength: $\lambda \simeq 0.5$ m - Penalty parameter: $\tau = 1$

HDG method	# DoF $\mathbf{\Lambda}$ field	# DoF EM field
HDG-$\mathbb{P}_1$	21,127,506	39,500,976
HDG-$\mathbb{P}_2$	42,255,012	98,752,440
HDG-$\mathbb{P}_3$	70,425,020	197,504,880

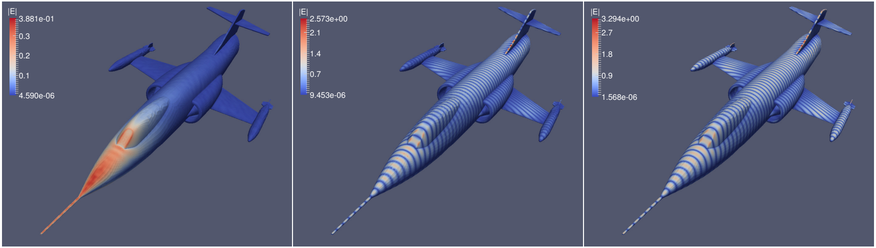

Contour line of $|\mathbf{E}|$ - HDG$-\mathbb{P}_1$ to HDG$-\mathbb{P}_3$

Scattering of a plane wave by a jet

- Unstructured tetrahedral mesh: 1,645,874 elements and 3,521,251 faces
- Fequency: 600 MHz - Wavelength: $\lambda \simeq 0.5$ m - Penalty parameter: $\tau = 1$
- Performance results: Occigen Bull/Atos cluster at CINES
  Intel E5-2690, 2.6 GHz, 24 cores on each node
  64 GB or 128 GB RAM per node

HDG method	# cores	# iter	Fact. Time	Sol. Time	Wall time	Speedup
HDG-$\mathbb{P}_1$	384	3	2.6 sec	3.7 sec	6.8 sec	1.0
-	768	4	0.8 sec	2.3 sec	3.4 sec	2.0
HDG-$\mathbb{P}_2$	384	10	16.7 sec	40.5 sec	58.7 sec	1.0
-	768	12	5.1 sec	21.5 sec	27.1 sec	2.2
HDG-$\mathbb{P}_3$	768	23	18.8 sec	102.1 sec	122.6 sec	1.0
	1536	26	5.1 sec	52.0 sec	58.7 sec	2.1

Strong scalability analysis: PDE-based Schwarz algorithm with PaStiX as a local solver

Scattering of a plane wave by a squadron of jets

- Unstructured tetrahedral mesh: 8,539,215 elements and 18,045,563 faces
- Fequency: 600 MHz - Wavelength: $\lambda \simeq 0.5$ m - Penalty parameter: $\tau = 1$

HDG method	# DoF $\mathbf{\Lambda}$ field	# DoF EM field
HDG-$\mathbb{P}_1$	108,273,378	204,941,160
HDG-$\mathbb{P}_2$	216,546,756	512,352,900
HDG-$\mathbb{P}_3$	360,911,260	1,024,705,800

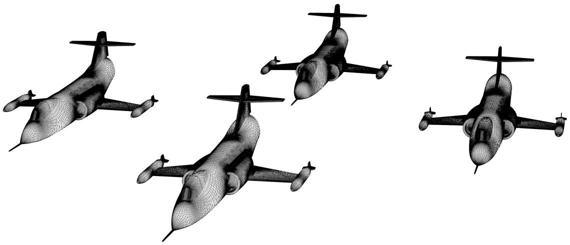

Scattering of a plane wave by a squadron of jets

- Unstructured tetrahedral mesh: 8,539,215 elements and 18,045,563 faces
- Fequency: 600 MHz - Wavelength: $\lambda \simeq 0.5$ m - Penalty parameter: $\tau = 1$

HDG method	# DoF $\boldsymbol{\Lambda}$ field	# DoF EM field
HDG-$\mathbb{P}_1$	108,273,378	204,941,160
HDG-$\mathbb{P}_2$	216,546,756	512,352,900
HDG-$\mathbb{P}_3$	360,911,260	1,024,705,800

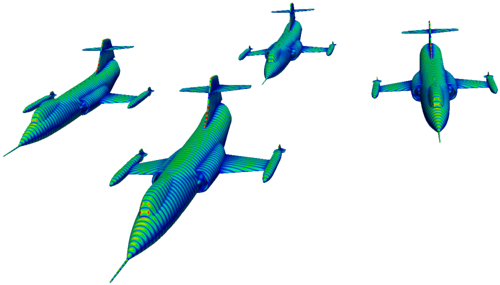

Scattering of a plane wave by a squadron of jets

- Unstructured tetrahedral mesh: 8,539,215 elements and 18,045,563 faces
- Fequency: 600 MHz - Wavelength: $\lambda \simeq 0.5$ m - Penalty parameter: $\tau = 1$
- Performance results: Occigen Bull/Atos cluster at CINES
  Intel E5-2690, 2.6 GHz, 24 cores on each node
  64 GB or 128 GB RAM per node

HDG method	# cores	# iter	Fact. Time	Sol. Time	Wall time	Speedup
HDG-$\mathbb{P}_1$	1536	2	4.4 sec	3.8 sec	9.0 sec	1.00
-	3072	3	1.7 sec	3.1 sec	5.1 sec	1.75
HDG-$\mathbb{P}_2$	1536	14	30.0 sec	85.0 sec	115.0 sec	1.00
-	3072	15	8.9 sec	40.0 sec	49.9 sec	2.30
HDG-$\mathbb{P}_3$	3072	28	34.0 sec	185.1 sec	221.6 sec	1.00

Strong scalability analysis: PDE-based Schwarz algorithm with PaStiX as a local solver

Outline

1. Context
2. Time-domain modeling
   - Brief history of the development of DGTD methods
   - DGTD methods for nanoscale light/matter interactions
3. Frequency-domain modeling
   - Hybridizable DG method
   - Scalable DD-based HDG solver
4. Closure

Closure

- Particular thanks to:
  - Stéphane Descombes (Professor Côte d'Azur University and Inria)
  - Clément Durochat (former PhD student, Inria)
  - Loula Fezoui (Senior research scientist, Inria)
  - Alexis Gobé (PhD student, Inria)
  - Raphaël Léger (fixed-term engineer, Inria)
  - Liang Li (Assistant professor, School of Mathematical Sciences, UESTC, China)
  - Ludovic Moya (former PhD student, then fixed-term engineer, Inria)
  - Claire Scheid (Assistant professor, Côte d'Azur University and Inria)
  - Nikolaï Schmitt (PhD student, Inria)
  - Jonathan Viquerat (former PhD student, then fixed-term engineer, Inria)

- Emmanuel Agullo, Luc Giraud and Matthieu Kuhn (Potsdoc)
  Hiepacs project-team, Inria Bordeaux-Sud Ouest
  Numerical linear algebra solvers
  PaStiX (sparse direct solver) and MaPHyS (algebraic DDM solver)

Closure

Ongoing and future works

- HDG method for frequency-domain treatment of plasmonic structures
  With Liang Li, School of Mathematical Sciences, UESTC, China
  In collaboration with Martijn Wubs, DTU Fotonik, Technical University of Denmark
- DG-based time-domain modeling of electron beam interaction with nanostructures
  PhD thesis of Nikolai Schmitt, ongoing
  In collaboration with Kurt Busch, Theoretical Optics & Photonics group
  Institut für Physik of Humboldt-Universität zu Berlin, Germany
- Exponential time integration schemes for grid-induced stiffness and high order DGTD method
  PhD thesis of Hao Wang (China Scholarship Council fellowship)
  In collaboration with Bin Li and Li Xu, School of Physical Electronics
  UESTC, Chengdu, China
- Reduced-order DGTD modeling
  With Kun Li and Liang Li, School of Mathematical Sciences, UESTC, China
- Multiscale DG method for time-domain Maxwell equations
  PhD thesis of Alexis Gobé, ongoing
  In collaboration with Frédéric Valentin, LNCC, Petropolis, Brazil

Thank you for your attention !

Nachos project-team

- Numerical methods and high performance algorithms for the numerical modeling of wave interaction with complex geometries/media
- Common project-team with J.A. Dieudonné Mathematics Laboratory
UMR CNRS 7351, Côte d'Azur University

Scattering of a plane wave by a PEC sphere of radius $r = 0.5$ m

- Incident plane wave angles: $\theta_{\text{inc}} = 90^\circ$ and $\phi_{\text{inc}} = 0^\circ$
- Fequency: 900 MHz - Wavelength: $\lambda \simeq 0.3333$ m - Penalty parameter: $\tau = 1$
- Artificial boundary: sphere of radius R
- RCS computation $\sigma_{\text{RCS}}(\theta, \phi)$ with $\theta = 90^\circ$ and $\phi = 0^\circ$ to 180°
- Parallel simulations performed on the PlaFRIM system
  - Nodes with 2 dodeca-core Intel Haswell Xeon E5-2680@2.5 GHz, RAM 128 GB
  - Simulations on 4 nodes and 96 cores
- Objective of the study
  - Validation of RCS computation
  - Reference solution from BEM solver (Airbus Group Innovations)
    CPU: 2 mn 30 sec on 8 cores
  - Influence of the distance between the object and the absorbing boundary
  - Absorbing boundary is a sphere of different radius
    $R = r + 1.5\lambda$, $r + 2\lambda$, $r + 3\lambda$ and $r + 4\lambda$ ($\Rightarrow$ 4 different meshes)

Scattering of a plane wave by a PEC sphere of radius $r = 0.5$ m

Local adaptation of the interpolation degree (9 points per wavelength): 52 sec

	# elements	# faces
	94,353	207,142
$\mathbb{P}_1$	12,977	18,667
$\mathbb{P}_2$	65,050	134,346
$\mathbb{P}_3$	16,195	39,778
$\mathbb{P}_4$	131	384

$r + 1.5\lambda$

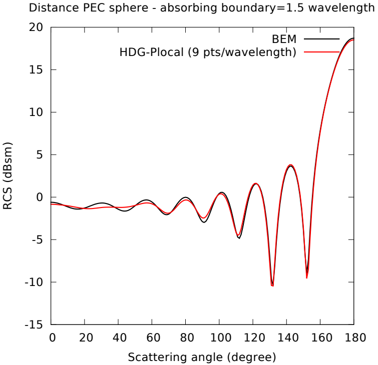

Scattering of a plane wave by a PEC sphere of radius $r = 0.5$ m

Local adaptation of the interpolation degree (9 points per wavelength): 1 mn 51 sec

	# elements	# faces
	119, 244	260, 716
$\mathbb{P}_1$	12, 920	18, 474
$\mathbb{P}_2$	70, 023	141, 995
$\mathbb{P}_3$	31, 943	71, 274
$\mathbb{P}_4$	4, 358	11, 967

$r + 2\lambda$

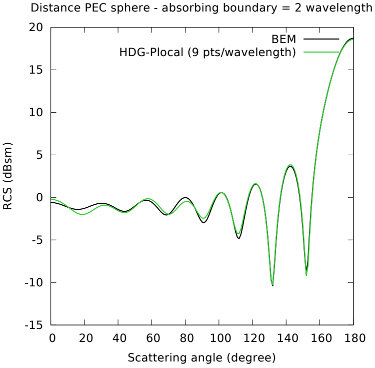

Scattering of a plane wave by a PEC sphere of radius $r = 0.5$ m

Local adaptation of the interpolation degree (9 points per wavelength): 5 mn 12 sec

	# elements	# faces
	203,597	439,311
$\mathbb{P}_1$	13,088	18,703
$\mathbb{P}_2$	93,106	176,087
$\mathbb{P}_3$	86,917	191,581
$\mathbb{P}_4$	10,486	28,314

$r + 3\lambda$

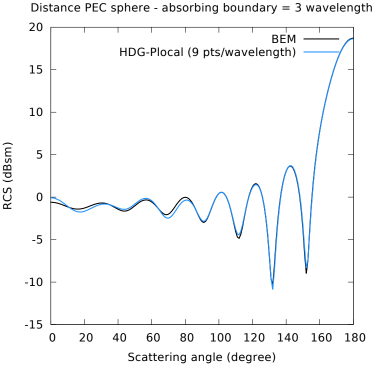

Scattering of a plane wave by a PEC sphere of radius $r = 0.5$ m

Local adaptation of the interpolation degree (9 points per wavelength): 8 mn 1 sec

	# elements	# faces
	334, 768	714, 939
$\mathbb{P}_1$	13, 525	19, 401
$\mathbb{P}_2$	125, 724	223, 466
$\mathbb{P}_3$	177, 914	388, 914
$\mathbb{P}_4$	17, 605	48, 236

$r + 4\lambda$